Electronic Excitations in Aggregates of Bacteriochlorophylls

Marshall G. Cory and Michael C. Zerner*

Department of Chemistry, University of Florida, Gainesville, Florida 32611

Xiche Hu and Klaus Schulten*

Beckman Institute and Department of Physics, University of Illinois at Urbana−Champaign, Urbana, Illinois 61801

Received: January 30, 1998; In Final Form: June 19, 1998

Photosynthetic organisms have developed antenna systems to enlarge their cross section for capturing sunlight. These systems involve in some cases aggregates of bacteriochlorophylls (BChls). The structure of one such aggregate, a tightly coupled circular hexadecamer of BChls and a loosely coupled octamer of BChls, has recently been solved. In this paper we investigate the electronic excitations in these two aggregates as well as in monomeric BChl and BChl dimers by means of INDO/S-CI calculations. The results provide a detailed description of the properties of electronic states in the BChl aggregates (energies, dipole and transition dipole moments) that are relevant for the biological function of BChls, to absorb light and transfer energy on the subpicosecond time scale. The lower-energy excitations of the BChl hexadecamer are of exciton type, i.e., experiencing a strong coupling that leads to excitation delocalization over the entire aggregate. An effective Hamiltonian is provided which reproduces these exciton states and which can be readily generalized to other aggregates.

1. Introduction

The light harvesting (LH) complexes of photosynthetic bacteria establish a scaffold which organizes a hierarchy of circular aggregates of, typically, 300 bacteriochlorophylls (BChls) and 200 carotenoids in the photosynthetic membranes of purple bacteria.[1,2] Shaped in the form of a ring, LH-I, the largest light harvesting complex, surrounds a central pigment−protein complex called the reaction center (RC). LH-I and the reaction center, in turn, are surrounded by about 10 smaller light harvesting complexes, called LH-II, which are also ring-shaped. The entire system, the photosynthetic unit, absorbs sunlight, transfers the excitation energy efficiently within a few picoseconds from the periphery to the reaction center, and converts the light energy, thereby, into a potential across the membrane.[3−7]

Recently, crystal structures of bacterial LH-II complexes from two species, *Rhodospirillum (Rs.) molischianum* and *Rhodopseudomonas (Rps.) acidophila*, have been determined.[8,9] The availability of these high-resolution crystal structures has stimulated research in an already very active field on both the experimental and the theoretical fronts.[6,10−19] Most recently, LH-I of *Rhodobacter (Rb.) sphaeroides* has been computationally modeled on the basis of the protein's high degree of homology to LH-II of *Rs. molischianum*.[6,12,20,21] The structures provide detailed information on the spatial organization of their chromophores and, thereby, can serve as a basis for a study of electronic excitations and excitation transfer based on *a priori* principles.[12,22,23]

LH-II from *Rs. molischianum*[8] is actually a circular aggregate of eight identical subunits. Each subunit contains a pair of short peptides, commonly referred to as the α-apoprotein and the β-apoprotein, noncovalently binding three bacteriochlorophyll-a (BChl-a) molecules and one lycopene. The subunits are called αβ-heterodimers. Figure 1 depicts the 24 BChl molecules in LH-II from *Rs. molischianum* with all other components stripped away. Sixteen of the BChls form a ring of 23 Å radius (based on central Mg atoms of BChls) in which the tetrapyrrole rings of each BChl partially overlap each other. The remaining eight BChls, forming a ring of 28 Å (radius), are arranged such that their tetrapyrrole rings are nearly perpendicular to the former (sixteen) BChls.

The main low-energy absorption band of BChls is the Q_y transition; the corresponding transition dipole moment lies along the molecular *y* axis connecting the N atom of pyrrole I with the N atom of pyrrole III (see Figure 1, refs 26, 27). In LH-II from *Rs. molischianum* this transition occurs at 800 nm as well as at 850 nm, suggesting that one of the BChl rings absorbs at 800 nm and the other at 850 nm. Given the structure of LH-II from *Rs. molischianum*, linear dichroism measurements suggest that the BChls forming the 23 Å ring absorb at 850 nm and the BChls forming the 28 Å ring absorb at 800 nm.[8,9]

The availability of an observed structure of the RC of *Rb. sphaeroides* and of structures of LH-I and LH-II of this species obtained by homology modeling provides an opportunity to assemble an entire light harvesting apparatus for this species made of the RC, an LH-I surrounding it, and several LH-II forming satellites around LH-I.[1,12,22] Figure 2 presents the aggregates of BChls in a section of this light harvesting system with all other components (protein and carotenoid) stripped away. Clearly, the circular organization of the BChl aggregates is a most intriguing feature of the bacterial light harvesting complexes. To understand how such aggregates serve the light harvesting function requires knowledge of the electronic properties of the excited states of the circular BChl aggregate.

In this paper we seek to describe the electronic states of the BChl aggregates in LH-II from *Rs. molischianum* on the bases

* Authors to whom correspondence should be addressed.

S1089-5647(98)00966-3 CCC: $15.00
Published on Web 09/09/1998

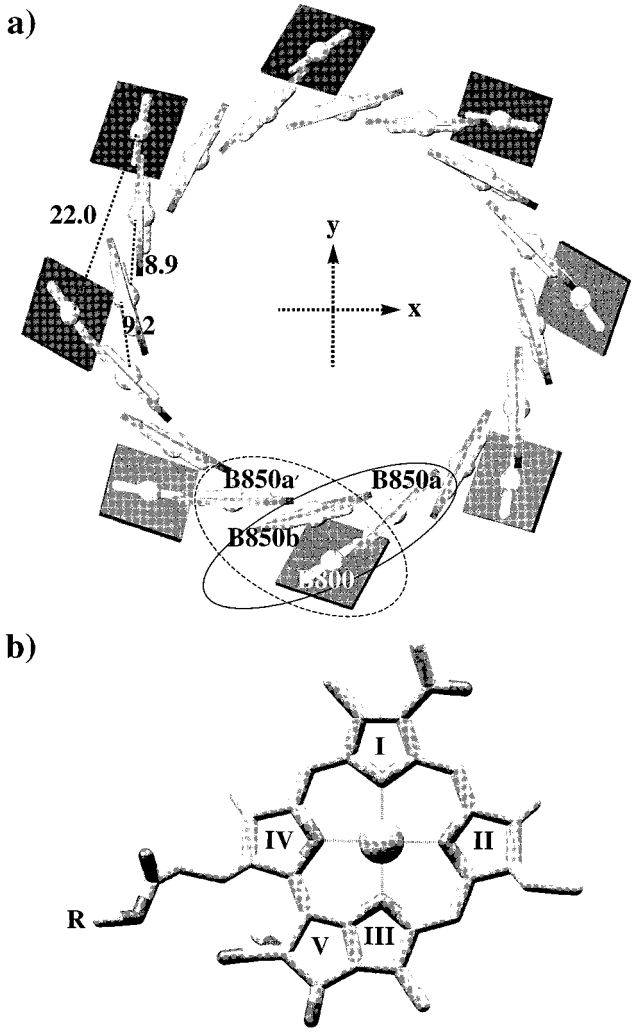

Figure 1. (a) Arrangement of bacteriochlorophylls in LH-II of *Rs. molischianum*.[8] Bacteriochlorophylls (BChls) are represented as squares; 16 B850 BChls (gray) are arranged in the inner ring and eight B800 BChls (black) in the outer ring. Bars connected with the BChls represent the Q_y transition dipole moments of individual BChls, and the van der Waals spheres show the position of the central Mg atoms of BChls. Representative distances between central Mg atoms of B800 BChl and B850 BChl are indicated (in Å). The Cartesian coordinate system is set up such that the 8-fold symmetrical axis of the LH-II complex coincides with the *z* axis, and the *x* and *y* axes are in the plane of the paper. (b) Bacteriochlorophyll-a molecule in a licorice representation with the phytyl tail (R) truncated for clarity. The pyrrole rings are labeled in accord with the Fisher nomenclature.[24] (This figure is produced with the program VMD.[25])

of *a priori* principles, i.e., without adjustable parameters. Such aggregates pose a serious challenge to quantum chemical calculations due to their large size. Ab initio calculations are not yet feasible. Various calculations of electronic excitations of BChls in LH-II have been reported in the literature, ranging from an effective Hamiltonian representation based on the point dipole treatment[12,18,19,28] to a more sophisticated point monopole treatment,[17] and to the quantum mechanical consistent-force-field/π-electron (QCFF/PI) approach.[10] The drawback of these approaches is that they contain adjustable parameters which may introduce properties that are a consequence of the parameters chosen or mask other properties not resulting from a specific parameter choice. A practical solution avoiding such parameters is to employ semiempirical models such as the intermediate neglect of differential overlap model parametrized for spectroscopy (INDO/S) as implemented in the ZINDO computer program package.[29] The INDO/S model has been parametrized at the singly excited configuration (interaction) level (CIS) to reproduce the spectra of simple chromophores such as benzene, pyridine, and diazenes.[30] INDO-CIS calculations have previously been successfully applied to studies of the electronically excited states of chromophores involved in the primary electron-transfer process in the photosynthetic reaction center.[31] We have carried out INDO-CIS calculations on the two independent BChl aggregates shown in Figure 2, the ring of B800 BChls and the ring of B850 BChls in LH-II of *Rs. molischianum* with eight and sixteen BChls, respectively, and report the results below.

Our objective has been to determine the nature of the low-energy electronic states of B850 BChl and B800 BChl aggregates of LH-II and the associated optical properties. For this purpose, INDO-CIS calculations have been performed on monomeric BChl, BChl dimers, the entire B800 ring of eight BChls, and the entire B850 ring of sixteen BChls. In addition, we provide an improved set of parameters for the effective Hamiltonian description suggested in refs 12, 22 and applied to the entire photosynthetic apparatus as shown in Figure 2.

The remainder of this article is organized as follows. Section 2 describes the INDO-CIS method and the various structural BChl aggregates investigated. Results are presented in Section 3, and conclusions are summarized in Section 4.

2. Methods

Quantum mechanical electronic structure calculations were performed using the intermediate neglect of differential overlap model parametrized for spectroscopy (INDO/S).[30−32] The INDO/S model has been used extensively by us and many others. A review of the underlying model Hamiltonian has been furnished in ref 33. The model is based on the original INDO model of Pople, Segal, and Santry[34,35] and is similar to the complete neglect of differential overlap (CNDO) model adopted for spectroscopy by Jaffe and Delbene.[36,37] The CNDO model, however, does not contain the one-center two-electron terms (Slater−Condon factors[38]) and, therefore, is not suitable for excited states of transition metal complexes, nor is it accurate in reproducing singlet−triplet splittings in most aromatic systems.

Most parameters of the theory come directly from atomic spectroscopy and are based on experimental ionization potentials, electron affinities, and the Slater−Condon two-electron integrals. An atom with a valence-based *s*, *p* basis is given a single resonance integral $\beta(s) = \beta(p)$, those with an *s*, *p*, and *d* basis, integrals with two different values $\beta(s) = \beta(p)$ and $\beta(d)$, and those with an *s*, *p*, *d*, and *f* basis, integrals with three different values $\beta(s) = \beta(p)$, $\beta(d)$, and $\beta(f)$. The resonance integrals are determined empirically from a database of molecules with well-established structures and optical properties.

2.1 Hartree−Fock INDO Self-Consistent-Field Method. The Hartree−Fock−Roothaan method[39,40] employed here describes electrons in molecular systems by the equation

$$\boldsymbol{FC} = \Delta \boldsymbol{C}\epsilon \tag{1}$$

where **F** is the Fock matrix which we express in the form

$$\mathbf{F} = \mathbf{h} + \mathbf{G} \tag{2}$$

Here **h** represents the one-electron operator, **G** the two-electron operator, and Δ the overlap matrix. In the basis of atomic functions $\{\chi_\nu\}$ the elements of the one-electron operator are

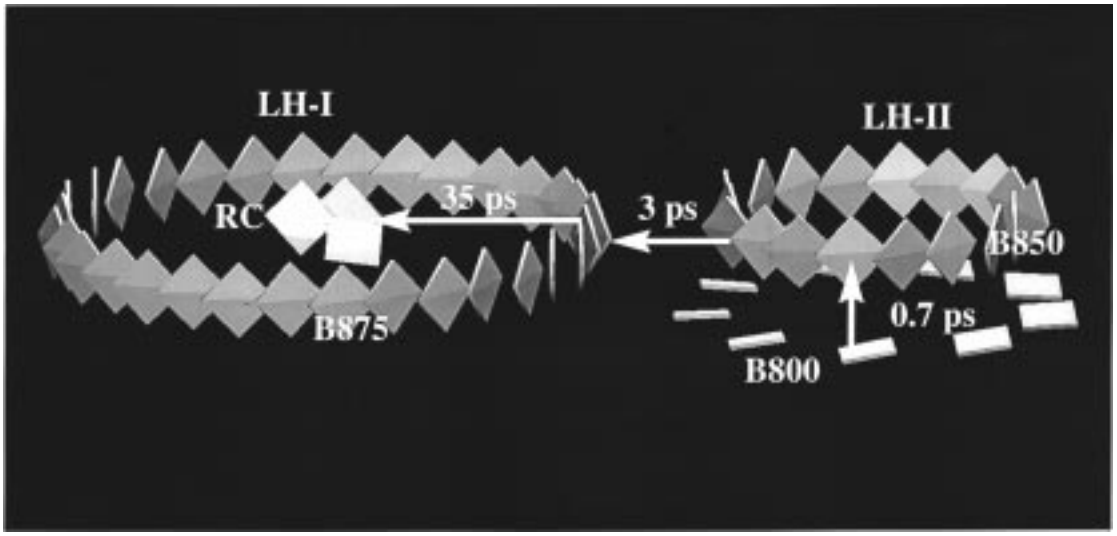

Figure 2. Geometrical relationship between BChls of LH-II and LH-I and the reaction center, RC, based on a model of the bacterial photosynthetic unit from *Rb. sphaeroides* obtained by homology modeling.[1,12] Observed[16] times for transfer of electronic excitation between the various components are shown. (This figure is produced with the program VMD.[25])

$$h_{\mu\nu} = \left\langle \mu \left| -\frac{1}{2}\nabla^2 - \sum_A \frac{Z_A}{R_A} \right| \nu \right\rangle \tag{3}$$

and the elements of the two-electron operator are given by the following expression which holds in the closed-shell case considered here

$$G_{\mu\nu} = \sum_{\rho\lambda} P_{\rho\lambda} \left\{ (\mu\nu|\rho\lambda) - \frac{1}{2}(\mu\rho|\nu\lambda) \right\} \tag{4}$$

We have introduced above the notation

$$(\mu\nu|\rho\lambda) = \int \mathrm{d}\tau_1 \int \mathrm{d}\tau_2 \, \chi_\mu(1)\, \chi_\nu(1) \frac{1}{r_{12}} \chi_\rho(2)\, \chi_\lambda(2) \tag{5}$$

The molecular orbitals ϕ_i are defined formally through the expansion coefficients $C_{\nu i}$

$$\phi_i = \sum_\nu \chi_\nu \, C_{\nu i} \tag{6}$$

In the INDO model, the basis set consists of an atomic set of valence orbitals only; the existence of inner-shell, i.e., core, electrons is accounted for through the parameters characterizing the INDO model Hamiltonian. In the closed-shell case all orbitals are either unoccupied or doubly occupied; i.e., the orbitals ϕ_i have occupancies η_i with values 0 or 2. The elements of the first-order Fock−Dirac density matrix **P** in eq 4 are then

$$P_{\mu\nu} = \sum_i C_{\mu i} \, C_{\nu i} \, \eta_i \tag{7}$$

In the following we denote by A, B atoms and by $S(J)$ the set of indices labeling orbitals on atom $J = A, B$.

In the INDO model, the diagonal matrix elements of **h** and **G** are given by ($\mu \in S(A)$)

$$h_{\mu\mu} = U_{\mu\mu} - \sum_{B,B\neq A} \sum_{\nu\in S(B)} Z_B^c (\bar{\mu}\bar{\mu}|\bar{\nu}\bar{\nu}) \tag{8}$$

$$G_{\mu\mu} = \sum_{\rho,\lambda\in S(A)} P_{\rho\lambda} \left[(\mu\mu|\rho\lambda) - \frac{1}{2}(\mu\rho|\mu\lambda) \right] + \sum_{B,B\neq A} \sum_{\rho\in S(B)} P_{\rho\rho} (\bar{\mu}\bar{\mu}|\bar{\rho}\bar{\rho}) \tag{9}$$

In eq 8 the approximation

$$\left(\mu \left| \frac{1}{R_B} \right| \mu \right) = (\bar{\mu}\bar{\mu}|\bar{\nu}\bar{\nu}) \tag{10}$$

is made. Z_A is the atomic number of atom A and Z_A^C is the core charge of atom A, i.e., Z_A^c equals the number of valence electrons, (4 for carbon, 8 for iron, etc); an overline indicates that only the spherically symmetric part of the integral is maintained. Z_A^c replaces Z_A in the INDO Hamiltonian since the core electrons have been assumed to completely screen the nuclear charge Z_A. The "core" integral $U_{\mu\mu}$ is an atomic property which can be determined empirically from ionization potentials.[38,41] The one-center two-electron integrals $(\mu\nu|\rho\lambda)$, with $\mu, \nu, \rho, \lambda \in S(A)$, are taken from experimental Slater−Condon radial integrals F^k and G^k determined by atomic spectroscopy.[30,38] The one-center off-diagonal matrix elements, i.e., for indices $\mu, \nu \in S(A)$, are given by

$$h_{\mu\nu} = 0 \tag{11}$$

$$G_{\mu\nu} = \sum_{\rho,\lambda\in S(A)} P_{\rho\lambda} \left[(\mu\nu|\rho\lambda) - \frac{1}{2}(\mu\rho|\nu\lambda) \right] \tag{12}$$

The off-diagonal elements of **h** and **G**, for $\mu \in S(A)$, $\nu \in S(B)$, $A \neq B$, are

$$h_{\mu\nu} = \frac{1}{2}(\beta_{\mu A} + \beta_{\mu B}) \, \bar{\Delta}_{\mu\nu} \tag{13}$$

$$G_{\mu\nu} = -\frac{1}{2} P_{\mu\nu} (\bar{\mu}\bar{\mu}|\bar{\nu}\bar{\nu}) \tag{14}$$

where the resonance integrals $\beta_{\mu A}$, $\beta_{\mu B}$ are empirical factors chosen to reproduce experimental spectra at the CIS level, and where $\bar{\Delta}_{\mu\nu}$ denotes a weighted overlap between atomic orbitals χ_μ and χ_ν. Further details are provided in ref 30, 33−35.

In carrying out the iterative SCF procedure, convergence proved to be a problem for the larger aggregates investigated. For such aggregates, the first cycle generates a molecular orbital manifold with nearly continuous, i.e., gapless, orbital energies resembling the half-filled energy band of a metal. The problem could be overcome by level shifting, a procedure in which the unoccupied orbitals are shifted according to the recipe

$$E(\text{level shift}) = 1.0 \text{ Hartree/SCF cycle number} \quad (15)$$

At the end of the tenth SCF cycle, the shifting is terminated. Failure to converge at this point was generally indicative of an error in the assumed geometry, as occurs readily for large systems. One must also be aware that such a procedure, especially in systems of high symmetry, can lock onto excited states.

For the CI expansion at the CIS level, one needs to evaluate the Hamiltonian in the basis of singly-excited electron configurations. For this purpose one can use the INDO/S Hamiltonian stated as in conventional many-electron theory

$$\hat{H} = \sum_{i,j}\sum_{\sigma}\tilde{h}_{ij}c^{\dagger}_{i\sigma}c_{j\sigma} + \frac{1}{2}\sum_{i,j,k,l}\sum_{\sigma,\sigma'}(ij\tilde{|}kl)\, c^{\dagger}_{i\sigma}c^{\dagger}_{k\sigma'}c_{l\sigma'}c_{j\sigma} \quad (16)$$

where the operators $c^{\dagger}_{i\sigma}$ ($c_{i\sigma}$) are fermion creation (annihilation) operators which create (annihilate) an electron in molecular orbital ϕ_i, as it results from the SCF calculation, and spin σ. Here $\tilde{h}_{ij}$ and $(ij\tilde{|}kl)$ denote the matrix elements of the single- and two-electron operators transformed into the basis of molecular orbitals ϕ_i. No further specification of INDO/S interaction parameters is needed for the many-electron problem stated in this form. The singly-excited electron configurations promoting an electron from occupied molecular orbital i (j) to unoccupied molecular orbital a (b), denoted by $|i \rightarrow a\rangle$ ($|j \rightarrow b\rangle$), are coupled to a singlet overall spin state and serve as the basis of the CIS calculation. The elements of the Hamiltonian (eq 16) in this basis are

$$\langle i \rightarrow a|\hat{H}|j \rightarrow b\rangle = \underbrace{(\varepsilon_a - \varepsilon_i)}_{\Delta\varepsilon}\delta_{ij}\delta_{ab} - \underbrace{\langle ij\tilde{|}ab\rangle}_{J} + 2\underbrace{\langle ia\tilde{|}jb\rangle}_{K} \quad (17)$$

where ϵ_i, etc., are the eigenvalues of the SCF matrix associated with ϕ_i etc. The symbols $\Delta\epsilon$, J (Coulomb integral), and K (exchange integral) refer to Figure 3 which compares various energy contributions for the excitations constructed on the basis of the four-orbital model, the latter being explained below.

The HF-INDO-SCF theory described above determines the ground-state reference energy and provides the set of molecular orbitals which are employed in the CIS calculation to determine excited state energies and transition dipole moments. The oscillator strengths f_n for the transition ground state $\rightarrow$ nth excited state are calculated from the transition dipole moments, including all one- and two-center terms of the transition dipole operator $\vec{\mu}$, according to the formula

$$f_n = 4.709 \times 10^{-7}\,(E_n - E_0) \times |\langle\psi_0|\vec{\mu}|\psi_n\rangle|^2 \quad (18)$$

where the energies E_n and E_0 are in units of cm^{-1} and $|\langle\psi_0|\vec{\mu}|\psi_n\rangle$ is in Debye. ψ_0 denotes the SCF ground state, and ψ_n describes the nth eigenstate of the CIS Hamiltonian given by

$$\psi_n = \sum_{i,a} d^{(n)}_{ia}\,|i \rightarrow a\rangle \quad (19)$$

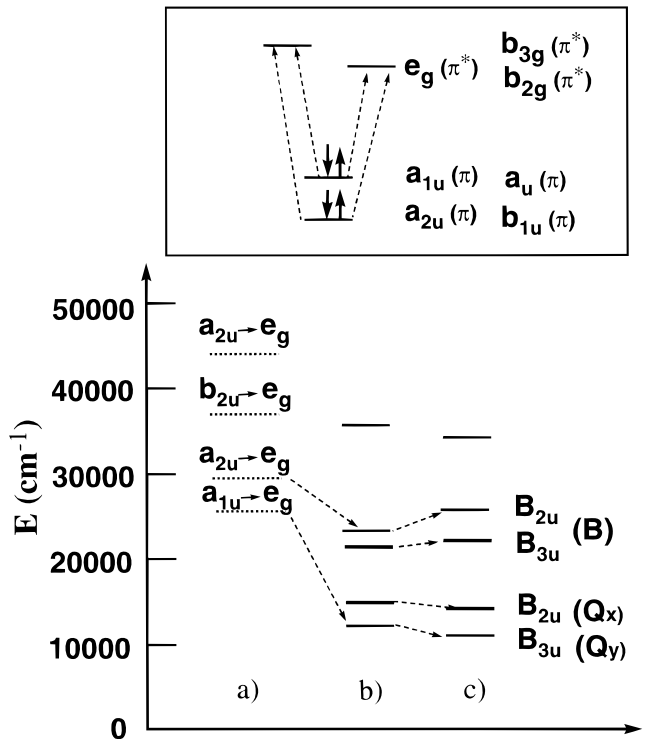

Figure 3. Four-orbital model for Bchl.[26,49] The orbitals (see text) are denoted by the D_{4h} labels for porphyrin as well as by the respective D_{2h} labels.[48] The four single excitations, which can be constructed in the four-orbital model, are shown. Their energies are given at three levels of description: (a) difference of molecular orbital energies, i.e., the term $\Delta\epsilon$ for the respective diagonal element of the CIS Hamiltonian (eq 17); (b) the complete respective diagonal element of the CIS Hamiltonian (eq 17) $\Delta\epsilon - J + 2K$; (c) the energy resulting from the CIS calculation, i.e., the energy of the eigenstate (eq 19) of the CIS Hamiltonian with the respective single excitation $|i \rightarrow a\rangle$ as its major contribution.

The effects of the surrounding media are included, when required, using the self-consistent reaction field approach (SCRF) described in refs 41−43. This involves adding the response of the dielectric medium to the Fock operator according to the expression

$$F_{\mu\gamma} = F^{o}_{\mu\gamma} - [(\epsilon - 1)/(2\epsilon + 1)]a^{-3}\vec{\mu}_o \cdot \langle\mu|\vec{r}|\gamma\rangle \quad (20)$$

where $\vec{\mu}_o$ is the ground-state dipole moment, obtained iteratively, and where ϵ is the dielectric constant.[44,45] For our description we assume a cavity radius determined through mass density according to $a = 1.383\,(M_m/d)^{1/3}$, where M_m is the molar mass in g/mol, d is the density in g/mL, and a is in Bohr. To describe the effect of the protein environment, a dielectric constant $\epsilon = 9$ is assumed together with an effective refraction index of $n = \sqrt{2}$; the latter values have been suggested in ref 46.

We used for the structure of the various BChl aggregates the symmetrized coordinates of LH-II from *Rs. molischianum*.[8] Generally, if poor geometries are used in a quantum chemistry procedure, this becomes apparent either in the failure of the SCF procedure or yields results that are impossible to understand. Unreasonably long or short bond lengths, atoms too close to one another, unsaturated valencies, or the incorrect position of hydrogen atoms are easily discovered. We note, however, that the potential for serious error is present if poor geometries pass these tests, and the results are not obviously wrong. In the present study, in which there is an apparent high symmetry, the chances of errors are greatly reduced once the structure of one of the chromophores is correct.

TABLE 1: Spectrum of BChl-a Monomer Calculated by Means of the INDO-CIS Method in the Gas Phase and in a Dielectric Medium with $\epsilon = 9$ and $n = \sqrt{2}$

	energy[a]			state dipole (Debye)			transition dipole (Debye)		
state	cm^{-1}	[nm]	osc. str.	*x*	*y*	*z*	*x*	*y*	*z*
0	0.0			7.33	−0.10	−0.11			
				(20.9)	(−0.18)	(−0.34)			
1	13 335	[751]	0.766	2.85	−0.67	−0.05	11.0	0.98	−0.15
	(12 853	[778])	(0.45)	(5.27)	(1.82)	(−3.02)	(−8.02)	(−2.86)	(1.16)
2	18 117	[552]	0.003	4.52	−0.02	−0.08	0.51	−0.34	0.01
	(18 464	[541])	(0.037)	(14.3)	(5.06)	(−4.28)	(−1.01)	(−0.15)	(1.80)
3	26 702	[374]	0.001	4.57	−0.60	3.73	0.26	−0.06	0.01
	(28 485	[351])	(0.800)	(19.5)	(6.85)	(−10.9)	(4.52)	(1.56)	(6.06)
4	29 593	[338]	1.937	1.54	0.71	−0.16	−1.66	11.67	−0.09
	(28 318	[353])	(0.382)	(15.0)	(7.56)	(−4.04)	(3.23)	(0.72)	(−4.21)
5	30 264	[330]	0.166	13.0	−3.42	−0.37	2.81	1.87	−0.52
	(28 956	[345])	(0.539)	(13.4)	(5.64)	(−2.86)	(2.42)	(0.40)	(−5.79)
6	31 175	[321]	0.660	6.79	0.82	−0.27	−2.52	6.19	0.51
	(29 710	[337])	(0.519)	(14.0)	(5.32)	(−3.99)	(−0.76)	(0.14)	(6.04)

[a] Values in parentheses are for dielectric medium, calculated using eq 20 following refs 43, 44.

The INDO-CIS description predicts the Q bands of porphyrin-like systems generally within 1000 cm^{-1},[31,33,47] i.e., quite accurately, and these are the bands of photochemical interest in these systems. The B bands (or Soret bands) are generally predicted some 4000−5000 cm^{-1} too high in energy by CIS calculations.[47,48] This is a consequence of the failure of the simple four-orbital model (see Figure 3) to describe the B bands: double excitations are required to lower the calculated energy and to reduce the calculated oscillator strength. However, the present study focuses on the lower excitations and, accordingly, CIS level calculations should be of sufficient accuracy for our purpose.

2.2 Aggregates Modeled. Before introducing the BChl aggregates to be investigated, it is useful to review some salient features of the underlying structure of LH-II from *Rs. molischianum*.[8] LH-II from *Rs. molischianum* exhibits C_8 symmetry.[8] As shown in Figure 1, each $\alpha\beta$-heterodimer contains three BChls: B800, B850a, and B850b (in the ellipse enclosed by a solid line). We denote by B850a the B850 BChl binding to the α-apoprotein, and by B850b the B850 BChl binding to the β-apoprotein (see Figure 1). Bacteriochlorophyll B850a′ is bound to the α-apoprotein of the (left) neighboring heterodimer. The Mg−Mg distances between B850a and B850b measure 9.2 Å, the Mg−Mg distances between B850a′ and B850b measure 8.9 Å. Mg−Mg distances between neighboring B800 BChls measure 22 Å.

LH-II from *Rs. molischianum* contains an aggregate of 24 BChls, composed of the strongly coupled aggregate of 16 B850 BChls and the more weakly coupled aggregate of eight B800 BChls. The aggregates studied are the following:

(i) BChl monomer;

(ii) B850 BChl dimers; dimer A with B850a and B850b (i.e., chromophores surrounded by the solid ellipse in Figure 1), and dimer B with B850a′ and B850b (i.e., chromophores surrounded by the dashed-line ellipse in Figure 1);

(iii) the B800 octamer, created from the structure of LH-II of *Rs. molischianum* by truncating each chromophore to 44 atoms, and generating a structure with exact C_8 symmetry; the latter is difficult to do, even in double precision algebra; artificial splitting can easily occur in case of imperfect symmetry, especially in the E_2 levels;

(iv) the B850 hexadecamer, created from the structure of LH-II of *Rs. molischianum* by truncating each chromophore to 44 atoms, and generating a structure with exact C_8 symmetry; the B850 hexadecamer includes 704 atoms and over 2000 electrons; the CI expansion included 4096 configurations for each of the A and B representations of the group corresponding to the symmetry of the aggregate.

3. Results and Discussion

BChl Monomer. To establish a point of reference we consider first the properties of a BChl monomer. The calculated properties are presented in Table 1. Figure 3 exhibits, schematically, the involvement of four BChl orbitals in the lowest energy excitations, two occupied π orbitals of $a_u(\pi)$ and $b_{1u}(\pi)$ symmetry in D_{2h} and two unoccupied π orbitals of $b_{2g}(\pi^*)$ and $b_{3g}(\pi^*)$ symmetry. Excitations between these four orbitals (the four-orbital model[26,49]) give rise to two transitions of *y* symmetry (i.e., transition dipole moment in the *y* direction) and two of *x* symmetry (transition dipole moment in the *x* direction). The lowest two excitations are labeled Q_y ($^1B_{2u}$) and Q_x ($^1B_{3u}$) and are calculated to lie at 13 335 and 18 117 cm^{-1}, respectively. The Q_y excitation is characterized by a transition dipole moment along the *y* axis which passes through the two opposite, reduced pyrrol rings in the case of D_{2h} bacteriochlorin; in the case of BChl the transition dipole moment is slightly rotated (see Table 1 for bacteriochlorophyll). The two upper transitions of these four are the principal components of the Soret or B band [B_y ($^1B_{2u}$) and B_x ($^1B_{3u}$)], that we predict at 26 702 and 29 593 cm^{-1}. As mentioned previously, the four-orbital description is reasonably accurate for the Q bands, but higher excitations, including double and triple excited configurations, affect B. The INDO/CIS model generally calculated the B bands 4000−5000 cm^{-1} too high in energy. This is also the case here.

It is informative to compare the stated results with those of D_{4h} porphyrins, in which rings I−IV are all pyrrol rings. In this case the occupied orbitals are the nearly degenerate pair $a_{1u}(\pi)$ and $a_{2u}(\pi)$, and the unoccupied orbitals are the degenerate $e_g(\pi^*)$ pair (see Figure 3). The four-orbital model then produces two nearly degenerate, optically intense ^1E_u transitions, which mix strongly through CI, producing the relatively weak Q bands [$E(Q_x) = E(Q_y)$ in D_{4h}] and the very intense B bands [$E(B_x) = E(B_y)$ in D_{4h}]. The reduction in symmetry in the formation of chlorins splits the degeneracy not only of each of the ^1E_u transitions (into $^1B_{2u}$ and $^1B_{3u}$), but also separates the two predicted $^1B_{2u}$ and $^1B_{3u}$ excitations. Because these pure configurations are separated significantly in energy, the excitations do not mix much in the CI description. Both the Q and the B states remain strongly allowed. This is important for

TABLE 2: Spectrum of BChl-a Dimers Calculated by Means of the INDO-CIS Method in the Gas Phase and in a Dielectric Medium with $\epsilon = 9$ and $n = \sqrt{2}$; Dimers are Defined in Figure 1

	energy[a]			state dipole (Debye)			transition dipole (Debye)		
state	cm^{-1}	[nm]	osc. str.	*x*	*y*	*z*	*x*	*y*	*z*
				Dimer A ($R_{Mg-Mg} = 9.2$ Å)					
0	0.0			2.14	8.23	−4.20			
				(0.82)	(9.84)	(−5.36)			
1	12 040	[831]	1.25	4.06	7.80	−4.20	−13.6	7.54	−0.09
	(12 025)	([832])	(1.38)	(3.19)	(9.18)	(−5.35)	(13.6)	(−7.64)	(0.07)
2	13 452	[743]	0.08	0.46	10.1	−3.98	1.63	−2.94	−0.96
	(13 431)	([745])	(0.07)	(0.08)	(11.08)	(−5.17)	(−1.33)	(2.79)	(0.94)
3	16 179	[618]	0.001	−41.1	15.1	−5.47	0.01	−0.25	−0.10
	(14 815)	([675])	(0.001)	(−41.6)	(16.2)	(−6.65)	(0.00)	(−0.26)	(−0.10)
4	17 637	[567]	0.001	32.1	4.23	−3.76	−0.38	−0.03	0.10
	(17 133)	([584])	(0.001)	(28.4)	(5.87)	(−4.91)	(−0.40)	(0.00)	(0.11)
				Dimer B ($R_{Mg-Mg} = 8.9$ Å)					
0	0.0		7.92	7.04	−5.78				
			(8.53)	(8.33)	(−7.49)				
1	12 157	[822]	1.25	7.85	5.22	−5.70	8.00	12.40	−0.16
	(12 131)	([824])	(1.22)	(8.83)	(5.77)	(−7.39)	(−7.91)	(12.3)	(−0.22)
2	13 359	[749]	0.18	4.77	8.94	−5.66	−5.17	0.61	0.90
	(13 335)	([750])	(0.18)	(5.24)	(10.22)	(−7.37)	(−5.24)	(0.73)	(0.87)
3	15 842	[631]	0.002	40.8	−9.93	−5.80	0.07	0.57	0.00
	(14 229)	([703])	(0.005)	(41.49)	(−9.08)	(−7.46)	(−0.08)	(0.83)	(0.00)
4	16 331	[612]	0.001	−29.7	24.4	−4.29	0.10	−0.36	−0.02
	(15 920)	([628])	(0.001)	(−28.5)	(25.1)	(−5.98)	(−0.03)	(0.28)	(0.02)

[a] Values in parentheses are for dielectric medium, calculated using eq 20 following refs 43, 44.

photosynthetic systems since the latter favor the low-lying bands to be intense, both for greater absorption probability and for efficient energy transfer between the component chromophores.

The protein environment has a considerable effect on the spectral properties of chromophores. In the present study we account for this environment as outlined in Methods. The calculations predict for the Q_y transition a red shift from 751 to 778 nm and a 70% reduction of its oscillator strength.

The BChl monomers experience a considerable change in their dipole moments upon electronic excitation.

B850 Dimer. The spectra for both dimer A and dimer B (see Methods) evaluated by means of the INDO-CIS method are listed in Table 2. We recall that dimers A, B describe the two types of BChl pairings which occur in the B850 aggregate of LH-II. Dimer B corresponds to a structure that is similar to that observed in the reaction center special pair and has a Mg−Mg distance of 8.9 Å; dimer A has a longer Mg−Mg distance, i.e., 9.2 Å, and exhibits also a different relative arrangement of the two BChls, in that ring III and ring V of one BChl overlap with those of the other BChl in the opposite direction.

The four-orbital model (see Figure 3), in case of BChl dimers, leads to 16 relevant electron configurations: eight intra-BChl single excitations and eight inter-BChl single excitations; linear combinations of the former excitations are called exciton-type excitations, and those of the latter type are called charge resonance type excitations. The (energy-wise) lowest four of all these excitations, presented in Table 2, are of Q_y type; the lowest two of these are excitonic, the upper two are of charge resonance type. The effect of the dielectric medium on the energies of the excitonic states is small. However, the resonant charge transfer type excitations are strongly affected by the dielectric environment, e.g., the third excitation in dimer A (B) is red-shifted 618 nm → 675 nm (631 nm → 703 nm).

There occurs an important mixing of the lowest excitonic state with the upper charge resonance state (as it arises from electron configurations within the four-orbital model) that leads to an anomalous energy lowering of this exciton state relative to the other exciton states. Such a shift, though somewhat stronger, arises also in the special pair of the RC. It had been argued that this energy lowering ensures that the lowest Q_y excitation in the RC occurs in the special pair, such that excitation energy is trapped in this moiety for use in the primary charge separation.[50]

TABLE 3: Spectrum of B800 Octamer Calculated by Means of the INDO-CIS Method in the Gas Phase[a]

	energy		
state	cm^{-1}	[nm]	osc. str.
	Q_y		
1	13 148	[761]	0.26
2	13 208	[757]	3.34
3	13 208	[757]	3.34
4	13 307	[752]	0.00
5	13 307	[752]	0.00
6	13 378	[748]	0.00
7	13 378	[748]	0.00
8	13 403	[746]	0.00
	Q_x		
9	17 930	[558]	0.01
10	17 930	[558]	0.015
11	17 930	[558]	0.015
12	17 931	[558]	0.00
13	17 931	[558]	0.00
14	17 932	[558]	0.00
15	17 932	[558]	0.00
16	17 932	[558]	0.00

[a] The geometry of the octamer corresponds to that of the ring of B800 BChls in LH-II of *Rs. molischianum* as reported in ref 8.

An alternative view of the effect of dimerization focuses on the Q_y excitation of monomeric BChl. In the case of the dimer in a dielectric medium, the dimerization splits this excitation for dimer A (B) into two excitations, namely, 778 nm → 832 nm + 745 nm (→ 824 nm + 750 nm).

B800 Octamer. Table 3 presents the excited-state energies and transition dipole moments for the ring of eight B800 BChls of *Rs. molischianum* evaluated in the gas phase. Two narrow bands of excitations are shown, a band of Q_y excitations around 752 nm and a band of Q_x excitations around 558 nm. One may fit the levels of the Q_y and Q_x bands by the progression of energy

TABLE 4: Lower Exciton Manifolds of B850 Hexadecamer as Calculated by Means of the INDO-CIS Method in the Gas Phase[a]

		energy			trans.dpl.mom.(Debye)		
state	symm.	cm^{-1}	[nm]	osc. str.	*x*	*y*	*z*
				$Q_{y,1}$			
1	A	11 698	[854]	0.002	0	0	−0.55
2	E_1	12 120	[825]	6.240	33.07	0.11	0
3	E_1	12 120	[825]	6.240	0.11	−33.07	0
4	E_2	12 636	[791]	0	0	0	0
5	E_2	12 636	[791]	0	0	0	0
6	E_3	12 949	[772]	0	0	0	0
7	E_3	12 949	[772]	0	0	0	0
8	B	13 048	[766]	0	0	0	0
				$Q_{y,2}$			
9	A	13 883	[723]	0.190	0	0	5.39
10	E_1	13 927	[718]	0.080	2.64	−2.30	0
11	E_1	13 927	[718]	0.080	−2.30	−2.64	0
12	E_2	14 040	[712]	0	0	0	0
13	E_2	14 040	[712]	0	0	0	0
14	E_3	14 161	[706]	0	0	0	0
15	E_3	14 161	[706]	0	0	0	0
16	B	14 213	[704]	0	0	0	0
				$Q_{y,3}$			
17	A	16 618	[602]	0	0	0	0.29
18	E_1	16 619	[602]	0.022	−1.04	1.29	0
19	E_1	16 619	[602]	0.022	1.29	−1.04	0
20	E_2	16 620	[602]	0	0	0	0
21	E_2	16 620	[602]	0	0	0	0
22	E_3	16 621	[602]	0	0	0	0
23	E_3	16 621	[602]	0	0	0	0
24	B	16 621	[602]	0	0	0	0
				$Q_{y,4}$			
25	A	17 468	[572]	0	0	0	−0.03
26	E_1	17 468	[572]	0.017	−0.59	1.31	0
27	E_1	17 468	[572]	0.017	−1.31	−0.59	0
28	E_2	17 469	[572]	0	0	0	0
29	E_2	17 469	[572]	0	0	0	0
30	E_3	17 471	[572]	0	0	0	0
31	E_3	17 471	[572]	0	0	0	0
32	B	17 471	[572]	0	0	0	0

[a] The geometry of the hexadecamer corresponds to that of the ring of B850 BChls in LH-II of *Rs. molischianum* as reported in ref 8.

levels

$$E(n,j) = a_j - 2b_j \cos\left(\frac{2\pi n}{8}\right) \quad n = 0, 1, \ldots 7 \qquad (21)$$

assuming a circular system of quantum states with C_8 symmetry and only nearest neighbor interactions. The band of Q_y excitations is matched by eq 21 with constants $a_1 = 13\,289$ cm^{-1} and $b_1 = 127$ cm^{-1} with a standard deviation of $\sigma_1 = 11$ cm^{-1}. The band of Q_x excitations, likewise, is matched by parameters $a_2 = 17\,931.3$ cm^{-1} and $b_2 = 1.15$ cm^{-1} with $\sigma_2 = 0.5$ cm^{-1}. In assigning these constants, we used more significant digits than are displayed in Table 3. The small $b_{1,2}$ values show that the bands of B800 excitations are very narrow, in fact, only of the order of thermal energies at physiological temperature ($k_BT \approx 200$ cm^{-1}). This implies that excitations in the B800 band are localized on individual BChls.

B850 Hexadecamer. Table 4 presents the main result of this paper, the excited-state energies and transition dipole moments for the B850 BChl aggregate of LH-II of *Rs. molischianum*. The excitations fall into a band $Q_{y,1}$ of eight exciton states built up from the lower-energy excitation of dimer A at 824 nm, a band $Q_{y,2}$ of eight exciton states built up from the higher-energy excitation of dimer A at 750 nm, and two bands ($Q_{y,3}$, $Q_{y,4}$) of resonant charge-transfer excitations. Each band contains a low-energy A state, a high-energy B state, and six pairwise degenerate states labeled E_1, E_2, E_3 in the symmetry group C_8.

TABLE 5: Average Excited State Energies of Higher Exciton Manifolds of B850 Hexadecamer as Calculated by Means of the INDO-CIS Method in the Gas Phase[a]

	average energy		
manifold	cm^{-1}	[nm]	bandwidth cm^{-1}
5	17 843	[560]	0.4
6	18 036	[554]	5.5
7	19 647	[508]	0.0
8	20 291	[492]	0.0
9	21 778	[459]	0.0
10	22 702	[440]	0.0
11	23 778	[420]	0.0
12	23 872	[418]	0.0
13	25 064	[398]	0.0
14	25 242	[396]	0.0
15	25 397	[393]	0.0
16	25 496	[392]	0.0
17	26 083	[383]	0.0
18	26 185	[381]	0.0
19	26 278	[380]	0.0
20	26 335	[379]	0.0
21	26 573	[376]	0.0
22	26 592	[376]	0.0
23	26 678	[374]	0.0
24	26 944	[371]	0.6
25	27 257	[366]	0.0
26	27 291	[366]	0.0
27	27 376	[365]	0.0
28	27 468	[364]	0.0
29	27 472	[364]	1.8
30	27 551	[362]	0.0

[a] Each manifold contains eight states whose excited state energies are averaged to yield the value shown.

The $Q_{y,1}$ band exhibits a noteworthy asymmetry; the B level lies about 100 cm^{-1} above the E_3 level, whereas the A level lies 420 cm^{-1} below the E_1 level. An analysis of the CI expansions of the respective states shows that the strong depression of the A level is due to interaction (level repulsion) with charge resonance states, in particular, the states contributing to the $Q_{y,4}$ band.

In the $Q_{y,1}$ band the E_1 states carry the main oscillator strength. The oscillator strength of the circular aggregate is enhanced by a factor of 8 compared to that of monomeric BChl. The transition dipole moments of the optically allowed E_1 states are oriented in the *x*,*y* plane which is parallel to the plane of the photosynthetic membrane, and only the E_1 states absorb radiation polarized in this plane. The increase in oscillator strength reflects the character of the excitonic states as coherent superpositions of single BChl Q_y excitations which can add up the individual transition dipole moments. Similarly, the lowest energy state, the A state, exhibits vanishing transition dipole moments in the *x*, *y* plane due to destructive interference of the local transition dipole moments.

The A states of all bands, and only these states, exhibit nonvanishing transition dipole moments in the *z* direction, a property which is also a reflection of the coherence properties of the excitonic states.

One may fit the levels of the $Q_{y,3}$ and $Q_{y,4}$ bands to the progression of energy levels described by eq 21. The respective parameters are $a_3 = 16619.8$ cm^{-1}, $b_3 = 0.75$ cm^{-1}; $a_4 = 17469.4$ cm^{-1}, $b_4 = 0.82$ cm^{-1}. The small b_3 and b_4 values imply a very weak coupling between local excitations.

Table 4 lists only the excited state properties for the lower four exciton manifolds. Results for the higher exciton manifolds

are presented in Table 5. Due to space limitation, only the average excited state energy is given for each manifold. Each manifold contains eight states. Unlike the lower four exciton manifolds shown in Table 4, the higher exciton manifolds have a very narrow bandwidth. As shown in Table 5, the spread of excitation energies within each manifold is no more than 5.5 cm^{-1}.

Effective Hamiltonian Description of Excitonic States. The $Q_{y,1}$ and $Q_{y,2}$ bands of the hexadecamer ring of B850 BChls contain 16 states with contributions mainly from intramolecular Q_y excitations. One may ask if these bands can be described by a Hamiltonian defined only in a basis of local excitations

$$|\alpha\rangle = \psi_1(g)\cdot\psi_2(g) \ldots \psi_{\alpha-1}(g)\, \psi_\alpha(Q_y)\psi_{\alpha+1}(g) \ldots \psi_{2N}(g) \tag{22}$$

where $\psi_j(g)$ describes the jth BChl in the electronic ground state and $\psi_\alpha(Q_y)$ describes the αth BChl in the Q_y excited state. $2N$ is the number of BChls in the aggregate, i.e., 16 in case of the B850 system of LH-II. The states $|\alpha\rangle$ may be assumed to form an orthogonal basis such that

$$\langle\alpha|\alpha'\rangle = \delta_{\alpha\alpha'} \tag{23}$$

The Hamiltonian in the basis (eq 22) for $k = 1, 2, \ldots 2N$ can be written in the general form

$$\hat{H} = \begin{pmatrix}
\epsilon & \upsilon_1 & W_{1,3} & W_{1,4} & \ldots & . & W_{1,2N-1} & \upsilon_2 \\
\upsilon_1 & \epsilon & \upsilon_2 & W_{2,4} & \ldots & . & W_{2,2N-1} & W_{2,2N} \\
W_{3,1} & \upsilon_2 & \epsilon & \upsilon_1 & \ldots & . & W_{3,2N-1} & W_{3,2N} \\
W_{4,1} & W_{4,2} & \upsilon_1 & \epsilon & \ldots & . & . & . \\
. & . & . & . & . & . & . & . \\
. & . & . & . & . & . & . & . \\
. & . & . & . & . & . & . & . \\
. & . & . & . & \ldots & \epsilon & \upsilon_2 & W_{2N-2,2N} \\
. & . & . & . & \ldots & \upsilon_2 & \epsilon & \upsilon_1 \\
\upsilon_2 & . & . & . & \ldots & W_{2N,2N-2} & \upsilon_1 & \epsilon
\end{pmatrix} \tag{24}$$

Here, ϵ represents the excitation energy of the Q_y state of an individual BChl. The parameters υ_1 and υ_2 account for nearest neighbor interactions between chromophores. The interactions W_{jk} must reflect the C_8 symmetry of the B850 aggregate ($N = 8$).

In the following, we try to determine a Hamiltonian (eq 24) such that the associated spectrum reproduces the $Q_{y,1}$ and $Q_{y,2}$ bands as described by the INDO-CIS method. However, rather than assuming that all elements of the Hamiltonian, within the bounds of symmetry, are adjustable parameters, we attempt a description in which we approximate the matrix elements W_{jk} in eq 24 through the dipole−dipole coupling interaction

$$W_{j,k} = C\left(\frac{\vec{d}_j\cdot\vec{d}_k}{r_{jk}^{\,3}} - \frac{3(\vec{r}_{jk}\cdot\vec{d}_j)\,(\vec{r}_{jk}\cdot\vec{d}_k)}{r_{jk}^{\,5}}\right) \tag{25}$$

Here, $\vec{d}_j$ represents unit vectors describing the direction of the transition dipole moments of the ground state → Q_y state transition of the jth BChl, and $\vec{r}_{jk}$ is the vector connecting the centers of BChl j with BChl k; C is a constant independent of j and k. Expression 25 is exact in the case of large separations of BChls j and k, in which case C is determined by the transition dipole moment of the Q_y transition of monomeric BChl. Presently, we want to assume that C and the three matrix elements ϵ, υ_1, and υ_2 are adjustable parameters of the Hamiltonian.

To determine the four parameters ϵ, υ_1, υ_2, and C, we postulate that Hamiltonian (eq 24) reproduces the "edges" of the $Q_{y,1}$ and $Q_{y,2}$ bands exactly; i.e., it reproduces the energies (in units cm^{-1}; see Table 4)

$$E_1 = 11\,698,\ E_8 = 13\,048,\ E_9 = 13\,883,\ E_{16} = 14\,213 \tag{26}$$

It can been shown, following ref 12 and exploiting the C_8 symmetry of the system under consideration, that these energies are related to ϵ, υ_1, υ_2, and $W_{j,k}$ through the analytic expressions

$$E_{1/16} = \epsilon + \frac{1}{2}\sum_{i=1}^{N-1}(W_{1,2i+1} + W_{2,2i+1}) \pm \frac{1}{2}\sqrt{[\sum_{i=1}^{N-1}(W_{1,2i+1} - W_{2,2i+1})]^2 - 4[\upsilon_1 + \upsilon_2 + \sum_{i=1}^{N-2}W_{1,2i+2}]^2}$$

$$E_{8/9} = \epsilon + \frac{1}{2}\sum_{i=1}^{N-1}(-1)^i\,(W_{1,2i+1} + W_{2,2i+1}) \pm \frac{1}{2}\sqrt{[\sum_{i=1}^{N-1}(-1)^i\,(W_{1,2i+1} - W_{2,2i+1})]^2 - 4[\upsilon_1 - \upsilon_2 + \sum_{i=1}^{N-2}(-1)^i\,W_{1,2i+2}]^2} \tag{27}$$

The coupling energies $W_{j,k}$ can be readily evaluated numerically according to eq 25 on the basis of the coordinates and transition dipole moments of the B850 BChls in LH-II of *Rs. molischianum*. One can determine then from eqs 26, 27 that $\epsilon = 13\,242\ cm^{-1}$, $\upsilon_1 = 790\ cm^{-1}$, $\upsilon_2 = 369\ cm^{-1}$, and $\upsilon_3 = -148\ cm^{-1}$. From υ_3 one can evaluate C using

$$C = \upsilon_3\left(\frac{\vec{d}_1\cdot\vec{d}_3}{r_{13}^{\,3}} - \frac{3(\vec{r}_{13}\cdot\vec{d}_1)(\vec{r}_{13}\cdot\vec{d}_3)}{r_{13}^{\,5}}\right)^{-1} \tag{28}$$

One finds C 505 644 $Å^3\ cm^{-1}$.

In ref 12 the parameters ϵ, υ_1, υ_2, and C had been determined on the basis of energies E_1, E_8, E_9, and E_{16} stemming from a smaller-scale INDO-CIS treatment of the B850 hexadecamer which employed actually only 512 configurations for each symmetry class, i.e., for A and for B symmetries. The values obtained in ref 12 differ only insignificantly from those stated above.

Table 6 compares the energies of the $Q_{y,1}$ and $Q_{y,2}$ band states as determined by means of the INDO-CIS method and by means of the effective Hamiltonian as described. One can recognize that the effective Hamiltonian reproduces qualitatively the $Q_{y,1}$ and $Q_{y,2}$ band energies, i.e., reproduces the sequence of A, E_1, E_2, E_3, B symmetry states, the wide bandwidth of 1350 cm^{-1} of the $Q_{y,1}$ band, the narrow bandwidth of 330 cm^{-1} of the $Q_{y,2}$ band, the gap of 835 cm^{-1} between the two bands, as well as the approximate spacing between the individual states. This is also demonstrated in Figure 4. One may note that the difference in the bandwidth of the $Q_{y,1}$ and $Q_{y,2}$ bands is due to the long-range interaction between the BChls, i.e., due to dipole−dipole coupling, and is not reproduced by an effective Hamiltonian with only nearest neighbor couplings υ_1 and υ_2; for the latter Hamiltonian the $Q_{y,1}$ and $Q_{y,2}$ bands have equal width $2\upsilon_2$ as can be seen readily from eq 27.

The effective Hamiltonian underestimates by a factor of 1/3 the gap between A and E_1 states which is calculated to be 422 cm^{-1} in the INDO-CIS description, but only 276 cm^{-1} in the

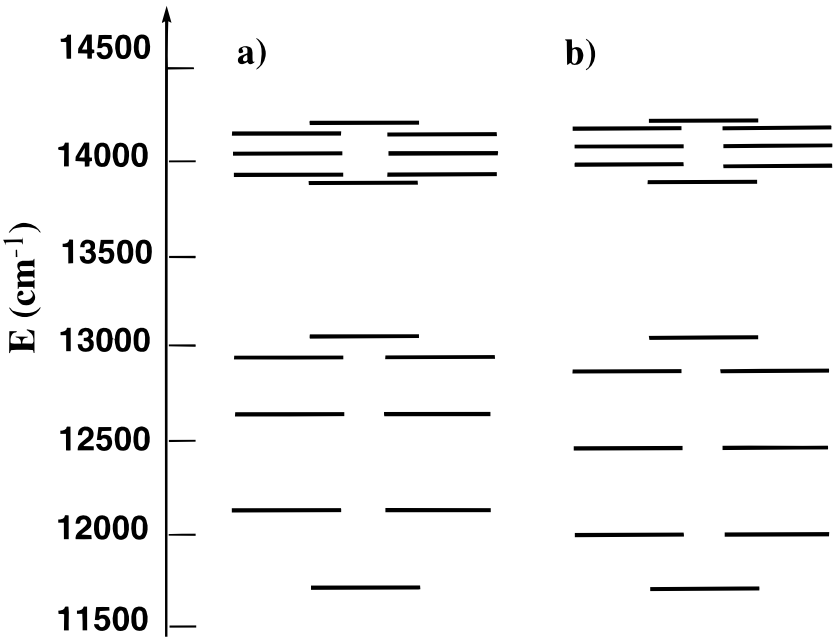

Figure 4. Spectrum of the circular hexadecameric aggregate of B850 BChls in the gas phase. (a) Results of INDO-CIS calculations (see Table 4); (b) spectrum as matched by the four-parameter effective Hamiltonian (eqs 24 and 25).

TABLE 6: Spectrum of B850 Hexadecamer Calculated by Means of the INDO-CIS Method in the Gas Phase and Calculated by Means of the Effective Hamiltonian as Explained in the Text[a]

state	symm.	energy cm^{-1} INDO-CIS	energy cm^{-1} eff. Ham.
		$Q_{y,1}$	
1	A	11 698	11 700
2	E_1	12 120	11 976
3	E_1	12 120	11 976
4	E_2	12 636	12 449
5	E_2	12 636	12 449
6	E_3	12 949	12 865
7	E_3	12 949	12 865
8	B	13 048	13 048
		$Q_{y,2}$	
9	A	13 883	13 884
10	E_1	13 927	13 962
11	E_1	13 927	13 962
12	E_2	14 040	14 088
13	E_2	14 040	14 088
14	E_3	14 161	14 176
15	E_3	14 161	14 176
16	B	14 213	14 210

[a] The geometry of the hexadecamer corresponds to that of the ring of B850 BChls in LH-II of *Rs. molischianum* as reported in ref 8.

effective Hamiltonian description. As pointed out above, the lowest exciton state is lowered in energy due to strong interactions with charge resonance states; these excitations are not included in the effective Hamiltonian description and, hence, this failure is to be expected.

The parameters characterizing the effective Hamiltonian are of interest. The value of ϵ is 93 cm^{-1} below the calculated energy of the Q_y state of monomeric BChl. This ϵ value implies that the individual BChls in LH-II have absorption maxima at 755 nm. It is intriguing that this site energy of 755 nm is nearly the same as the absorption maximum (772 nm) of BChl-a in organic solvent.[51] The difference in the values of v_1 and v_2 reflects the tighter coupling of B850a with B850b compared to that of B850a′ and B850b (see Figure 1). The tighter coupling between B850a and B850b BChls is expected since the tetrapyrrole rings of B850a and B850b BChls are geometrically more proximate than are those between B850a′ and B850b, although the latter pair displays a shorter Mg−Mg distance (8.9 Å) than the former pair (9.2 Å).[8] The value of C corresponds to a Q_y state transition dipole moment of 11 D (if one assumes an optical density $n = 1$). This value is larger than the previously estimated values of BChl in organic solvent which range from 6.1 D[52] to 7.7 D[53] (our value for the monomer in an $\epsilon = 9$ medium is 8.6 D, see Table 1). Given the simplicity of the effective Hamiltonian, the neglect of single excitations other than monomeric Q_y excitations, and the underlying assumption of an optical density of $n = 1$, the agreement of the oscillator strength within an error of 25% is actually an excellent result.

In this work, INDO-CIS calculations are carried out on the basis of coordinates of isolated BChl aggregates assuming a perfect C_8 symmetry. Since spectral properties of BChls are sensitive to their surroundings (protein, carotenoid, and lipids), an indigenous, glasslike disorder of the protein will perturb the symmetry of BChl rings. It is the extent of such perturbation that determines the nature of excitations of BChl aggregate which can be either delocalized or localized. In principle, the ratio of coupling strengths between BChls, i.e., v_1, v_2, to the magnitude of disorder determines the extent of delocalization. In the case of the B850 BChl aggregate, the effective coupling between nearest neighbor BChls is 790 cm^{-1} (v_1) within the $\alpha\beta$-heterodimer, and 369 cm^{-1} (v_2) between the $\alpha\beta$-heterodimers. Since these coupling strengths are larger than the magnitudes of disorder as estimated in refs. 12, 54, the electronic excitations of B850 BChls are most likely delocalized. This conclusion is consistent with results of a series of hole-burning and absorption spectroscopy experiments carried out by Small and co-workers.[13,55−58] A direct observation of the lowest exciton level (A) of the B850 BChl aggregate from LH-II of *Rps. acidophila* by absorption spectroscopy and by hole-burning spectroscopy at 4.2 K has been reported in ref 13. It was found that the strongly allowed E_1 state is responsible for the majority of the B850 absorption band, and the lowest exciton state (A) contributes to 3% of the total intensity of the B850 absorption band. The fact that the strongly allowed degenerate E_1 state

dominates the B850 absorption band suggests that electronic excitations of the B850 BChl aggregate is delocalized.

The hole-burning experiments reported in refs 13, 56, 57 provide an estimate of the splitting, ΔE, between the lowest state A and the strongly allowed E_1 state of the exciton system. A ΔE value of 290 cm^{-1} had been determined for LH-II from *Rs. molischianum*.[56] This value is smaller than the splitting of 422 cm^{-1} resulting from the present INDO-CIS calculations.

The discrepancy between the INDO-CIS ΔE value (422 cm^{-1}) and the experimentally estimated ΔE value of 276 cm^{-1} is considerable, and one must note that if the effect of disorder and temperature on ΔE is taken into account, the discrepancy would increase even further. As pointed out by Wu et al.,[57,58] the ΔE derived from the hole-burning spectroscopy is an apparent value that reflects the effects of disorder and the experimental temperature (4.2 K). It has been argued in ref 13 that ΔE increases with increasing disorder. For example, an apparent ΔE value of 200 cm^{-1} derived from hole-burning spectra for LH-II of *Rps. acidophila* is reduced to a real splitting (free of disorder) of 150 cm^{-1} when an experimentally acceptable level of diagonal energy disorder is taken into account.[13] Likewise, it has been argued that nearest neighbor couplings are much stronger at lower temperature ($T < 150$ K) based on an analysis of thermal broadening of the B850 absorption band.[13] From this it follows that the ΔE value derived from 4.2 K hole-burning spectra overestimates the excitonic splitting at room temperature.[13]

Further work at both the theoretical and experimental front is needed to resolve the described discrepancy in ΔE values. For example, in the analysis of hole-burning experiments ΔE is simply equated to center frequency displacement, which involves assumptions that need more careful scrutiny.[55,57] On the theoretical fronts, the point monopole treatment by Sauer et al. suggests actually a nearest neighbor coupling strength of 273 cm^{-1} for LH-II from *Rps. acidophila*,[17] which corresponds to a ΔE of about 100 cm^{-1} in a simple effective Hamiltonian scheme. However, the treatment in ref 17 is obviously more approximate than the INDO-CIS description presented here such that it does not resolve the existing discrepancy. The QCFF/PI approach by Alden et al. predicts ΔE values of 79 and 60 cm^{-1} for LH-II from *Rps. acidophila*, with and without disorder included, respectively.[10] Again, adjustable parameters are used in the QCFF/PI approach, which renders a direct comparison of the ΔE value by QCFF/PI with that of our INDO-CIS approach difficult since no adjustable parameter is used in the latter. Our experience with the INDO-CIS model is that disagreement with experiment may be related to physical defects in the modeled system, and that fitting directly to a specific experiment can hide these defects.

4. Conclusion

Photosynthetic life forms have developed various antenna systems to enlarge the cross section for capturing sunlight. The known systems all contain aggregates of chlorophylls (or bacteriochlorophylls) and of other chromophores.[6] In some cases, as in the light harvesting complexes of purple bacteria or in the chlorosomes of green bacteria,[59] tightly coupled aggregates of chlorophylls (or bacteriochlorophylls) are employed for this purpose, in other cases, as in dynoflagellates,[60] strongly coupled clusters of chlorophylls and carotenoids are used. Other photosynthetic life forms appear to utilize more weakly coupled chromophore aggregates. The ubiquitous nature of such aggregates in biological photosynthesis calls for a systematic investigation of their relevant electronic properties. The solution of the structures of light harvesting complexes has made computational investigations feasible.

The study of BChl aggregates presented in this paper is unique in that it does not rely on ad hoc parameters, but rather employs a model Hamiltonan, INDO/S,[29] for describing optical properties of molecules in general. This approach allows one to analyze, through the difference of calculated and observed spectra, how proteins control the spectral properties of bound BChls and to determine the effective couplings between aggregated BChls computationally without a priori coupling strengths. The results reported above for monomeric BChl suggest that such an approach can be successful. INDO-CIS calculations determine an absorption maximum of 751 nm in the gas phase and of 778 nm in a medium with $\epsilon = 9$ and $n = \sqrt{2}$. INDO-CIS calculations on trimers and hexamers of BChls (Zerner et al., unpublished results) attribute a 776−777 nm absorption to the B800 BChls, demonstrating that their spectral absorption is only very weakly coupled. The 776−778 nm values are close to the 800 nm value of B800 BChl in LH-II, indicating that the absorption of B800 BChl is not much affected through special ligation effects.

The INDO-CIS calculations reported above were remarkably successful in describing B850 BChls. The B850 BChl hexadecamer in LH-II of *Rs. molischianum* experiences a splitting of the (in vacuo) 751 nm Q_y level into 16 levels, associated with exciton type wave functions, which form two distinct bands, a wide lower-energy band and a narrow higher-energy band. Only two of the 16 exciton states, the pair of degenerate E_1 states (see Table 4), carry significant oscillator strength. These states are shifted to 825 nm relative to the 751 nm Q_y state of monomeric (in vacuo) BChl; i.e., the calculations reproduce well the red shift to 850 nm in LH-II of the spectrum of monomeric BChl upon forming the hexadecamer ring, in particular, if one considers that the dielectric properties of the protein could yield a further red shift by about 20 nm not yet accounted for by the gas-phase description. A crucial property of the B850 system in LH-II is the energy gap (ΔE) between the (energetically) lowest and second-lowest exciton level. The INDO-CIS calculation suggests a gap of 422 cm^{-1} which, given the degeneracy of the second-lowest state, implies an 82% occupancy of the lowest exciton state after thermal relaxation. Accordingly, the electronic properties of the lowest exciton state should govern the energy transfer characteristics of LH-II.

The INDO-CIS calculations predict, beside the lowest exciton levels, also two narrow bands of charge resonance character near 600 and 570 nm. These states are likely to experience a significant solvent shift as shown by the respective charge resonance state described in the BChl dimer. Spectroscopy might resolve these states and verify the present description.

Even though we stressed that the INDO-CIS description is free of ad hoc parameters, the establishment of an effective Hamiltonian model based on four adjusted parameters is one of the key accomplishments of the present investigation. The reason is that the effective Hamiltonian can be used much more easily than the INDO-CIS method and can be readily generalized to other BChl aggregates without the need of any further INDO-CIS treatment. The effective Hamiltonian might be employed to describe LH-II of *Rps. acidophila*[9] or of *Rb. sphaeroides*, light harvesting complex LH-I[12] and even the complete photosynthetic unit of purple bacteria as demonstrated in refs 1, 12, 22 (see Figure 2). One can also use the effective Hamiltonian to study the effect of disorder, i.e., the breaking of a perfect C_8 symmetry as done for static disorder in ref 12. The effective Hamiltonian has also the virtue of explaining the result of the

INDO-CIS method in terms of a relatively simple model; the parameters $\nu_1 = 790$ cm^{-1} ($\nu_2 = 369$ cm^{-1}) encapsulate the effective coupling between nearest neighbor BChls B850*a* and B850*b* (B850*a*′ and B850*b*).

The successful description of BChl aggregates by the INDO-CIS method encourages various new investigations. First, one may seek to include specific BChl−protein interactions with ligating and other proximate side groups. The good agreement between the results of this paper and spectral absorption features of BChl in LH-II suggest that specific interactions are not essential, but this supposition needs to be checked. Second, one may wish to extend the CIS treatment to include double excitations in order to describe pump−probe experiments populating double exciton states as discussed in ref 22. Third, one should extend the present description to other light harvesting systems with chlorophyll aggregates, e.g., to test the models suggested for aggregates in the chlorosomes of green bacteria.[59] Fourth, one may want to extend the simulations to describe complexes of carotenoids and BChls in LH-II or in the carotenoid-rich peridine−chlorophyll protein of dynoflagellates.[60] The present state of empirical modeling of the carotenoid−bacteriochlorophyll coupling as described, for example, in ref 23, calls urgently for INDO-type quantum chemical descriptions. Finally, the methodology applied to biological light harvesting can be extended to artificial light harvesting systems based on energy transfer in dendritic macromolecules as synthesized and probed in ref 61.

Acknowledgment. The authors thank A. Damjanović for carrying out effective Hamiltonian calculations. This work is supported in part through grants from the Carver Charitable Trust, the National Institutes of Health (P41RR05969), and the National Science Foundation (ASC9318159) (K.S.) and from NSW CHE as well as from the Office of Naval Research and National Science Foundation (CHE9312651) (M.C.Z.), and through an IBM SUR-96 Award.

References and Notes

(1) Hu, X.; Damjanović, A.; Ritz, T.; Schulten, K. *Proc. Natl. Acad. Sci. U.S.A.* **1998**, *95*, 5935.

(2) Papiz, M. Z.; Prince, S. M.; Hawthornthwaite-Lawless, A. M.; McDermott, G.; Freer, A. A.; Isaacs, N. W.; Cogdell, R. J. *Trends Plant Sci.* **1996**, *1*, 198.

(3) Lancaster, C. R. D.; Ermler, U.; Michel, H. In *Anoxygenic Photosynthetic Bacteria;* Blankenship, R. E., Madigan, M. T., Bauer, C. E., Eds.; Kluwer Academic Publishers: Dordrecht, The Netherlands, 1995; p 503.

(4) Parson, W. W.; Warshel, A. In *Anoxygenic Photosynthetic Bacteria*; Blankenship, R. E., Madigan, M. T., Bauer, C. E., Eds.; Kluwer Academic Publishers: Dordrecht, The Netherlands, 1995; p 559.

(5) Woodbury, N. W.; Allen, J. In *Anoxygenic Photosynthetic Bacteria*; Blankenship, R. E., Madigan, M. T., Bauer, C. E., Eds.; Kluwer Academic Publishers: Dordrecht, The Netherlands, 1995; p 527.

(6) Hu, X.; Schulten, K. *Phys. Today*, August, 1997, p 28.

(7) van Grondelle, R.; Dekker, J.; Gillbro, T.; Sundstrom, V. *Biochim. Biophys. Acta* **1994**, *1187*, 1.

(8) Koepke, J.; Hu, X.; Muenke, C.; Schulten, K.; Michel, H. *Structure* **1996**, *4*, 581.

(9) McDermott, G.; Prince, S.; Freer, A.; Hawthornthwaite-Lawless, A.; Papiz, M.; Cogdell, R.; Isaacs, N. *Nature* **1995**, *374*, 517.

(10) Alden, R.; Johnson, E.; Nagarajan, V.; Parson, W.; Law, C.; Cogdell, R. *J. Phys. Chem. B* **1997**, *101*, 4667.

(11) Meier, T.; Zhao, Y.; Chernyak, V.; Mukamel, S. *J. Chem. Phys.* **1997**, *107*, 3876.

(12) Hu, X.; Ritz, T.; Damjanović, A.; Schulten, K. *J. Phys. Chem. B* **1997**, *101*, 3854.

(13) Wu, H.-M.; Reddy, N. R. S.; Small, G. J. *J. Phys. Chem. B* **1997**, *101*, 651.

(14) Sturgis, J. N.; Olsen, J. D.; Robert, B.; Hunter, C. N. *Biochemistry* **1997**, *36*, 2772.

(15) Monshouwer, R.; van Grondelle, R. *Biochim. Biophys. Acta* **1996**, *1275*, 70.

(16) Pullerits, T.; Sundstrom, V. *Acc. Chem. Res.* **1996**, *29*, 381.

(17) Sauer, K.; Cogdell, R. J.; Prince, S. M.; Freer, A.; Isaacs, N. W.; Scheer, H. *Photochem. Photobiol.* **1996**, *64*, 564.

(18) Sturgis, J.; Robert, B. *Photosynth. Res.* **1996**, *50*, 5.

(19) Dracheva, T. V.; Novoderezhkin, V. I.; Razjivin, A. *FEBS Lett.* **1996**, *387*, 81.

(20) Hu, X.; Schulten, K. *Biophys. J.* **1998**, *75*, 683.

(21) Germeroth, L.; Lottspeich, F.; Robert, B.; Michel, H. *Biochemistry* **1993**, *32*, 5615.

(22) Ritz, T.; Hu, X.; Damjanović, A.; Schulten, K. *J. Lumin.* **1998**, *76*−*77*, 310.

(23) Damjanović, A.; Ritz, T.; Schulten, K. *Phys. Rev. E* **1998**, in press.

(24) Fisher, H.; Orth, H. *Die Chemie des Pyrrols*; Akademische Verlagsgesellschaft: Leipzig, 1937; Vol. 2. (Reprinted by Johnson Reprint Corp., New York, 1968.)

(25) Humphrey, W. F.; Dalke, A.; Schulten, K. *J. Mol. Graphics* **1996**, *14*, 33.

(26) Gouterman, M. *J. Mol. Spectrosc.* **1961**, *6*, 138.

(27) Weiss, C. *J. Mol. Spectrosc.* **1972**, *44*, 37.

(28) Hu, X.; Xu, D.; Hamer, K.; Schulten, K.; Koepke, J.; Michel, H. *Protein Sci.* **1995**, *4*, 1670.

(29) Zerner, M. C. *ZINDO, A General Semiempirical Program Package*; Department of Biochemistry, University of Florida: Gainesville, FL 32611.

(30) Ridley, J.; Zerner, M. *Theor. Chim. Acta* **1973**, *32*, 111.

(31) Thompson, M.; Zerner, M. *J. Am. Chem. Soc.* **1991**, *113*, 8210.

(32) Bacon, A. D.; Zerner, M. C. *Theor. Chim. Acta* **1979**, *53*, 21.

(33) Zerner, M. C. In *Reviews of Computational Chemistry, Vol. 2*; Lipkowitz, K. B., Ed.; VCH Publishing: New York, 1991; p 313.

(34) Pople, J.; Beveridge, D.; Dobash, P. *J. Chem. Phys.* **1967**, *47*, 2026.

(35) Pople, J.; Santry, D.; Segal, G. *J. Chem. Phys.* **1965**, *43*, 5129.

(36) DelBene, J.; Jaffe, H. H. *J. Chem. Phys.* **1968**, *48*, 1807.

(37) DelBene, J.; Jaffe, H. H. *J. Chem. Phys.* **1968**, *48*, 4050.

(38) Slater, J. C. *Quantum Theory of Atomic Structure, Vols. 1 and 2*, 1st ed.; McGraw-Hill: New York, 1960.

(39) Szabo, A.; Ostlund, N. S. *Modern Quantum Chemistry*, 1st ed.; Macmillan: New York, 1982.

(40) Pilar, F. L. *Elementary Quantum Chemistry*, 1st ed.; McGraw-Hill: New York, 1968.

(41) Karlsson, G.; Zerner, M. *Int. J. Quantum Chem.* **1973**, *7*, 35.

(42) Karelson, M. M.; Zerner, M. C. *J. Phys. Chem.* **1992**, *96*, 6949.

(43) Tamm, T.; Zerner, M. C., to be submitted for publication.

(44) Onsager, L. *J. Am. Chem. Soc.* **1936**, *58*, 1486.

(45) Kirkwood, J. *J. Chem. Phys.* **1934**, *2*, 351.

(46) King, G.; Lee, F.; Warshel, A. *J. Chem. Phys.* **1991**, *95*, 4366.

(47) Edwards, W. D.; Weiner, B.; Zerner, M. C. *J. Am. Chem. Soc.* **1986**, *108*, 2196.

(48) Edwards, W. D.; Zerner, M. C. *Int. J. Quantum Chem.* **1983**, *23*, 1407.

(49) Gouterman, M. *The Porphyrins, Vol. 3*; Academic Press: New York, 1978.

(50) Cory, M. G.; Zerner, M. C., to be submitted for publication.

(51) Oelze, J. *Methods Microbiol.* **1985**, *18*, 257.

(52) Sauer, K.; Smith, J. R. L.; Schultz, A. J. *J. Am. Chem. Soc.* **1966**, *88*, 2681.

(53) Pearlstein, R. M. *Photosynth. Res.* **1992**, *31*, 213.

(54) Wu, H.; Small, G. *J. Phys. Chem. B* **1998**, *102*, 888.

(55) Reddy, N. R. S.; Picorel, R.; Small, G. J. *J. Phys. Chem.* **1992**, *96*, 6458.

(56) Wu, H.; Reddy, N.; Cogdell, R.; Muenke, C.; Michel, H.; Small, G. *Mol. Cryst. Liq. Cryst.* **1996**, *291*, 163.

(57) Wu, H.; Ratsep, M.; Jankowiak, R.; Cogdell, R.; Small, G. *J. Phys. Chem. B* **1997**, *101*, 7641.

(58) Wu, H.; Ratsep, M.; Lee, I.; Cogdelli, R.; Small, G. *J. Phys. Chem. B* **1997**, *101*, 7654.

(59) Matthews, B.; Fenna, R.; Bolognesi, M.; Schmid, M. *J. Mol. Biol.* **1979**, *131*, 259.

(60) Hofmann, E.; Wrench, P.; Sharples, F.; Hiller, R.; Welte, W.; Diederichs, K. *Science* **1996**, *272*, 1788.

(61) Devadoss, C.; Bharathi, P.; Moore, J. *J. Am. Chem. Soc.* **1996**, *118*, 9635.